Hindawi
Mathematical Problems in Engineering
Volume 2023, Article ID 9944595, 10 pages
https://doi.org/10.1155/2023/9944595

Research Article

Mathematical Modeling of Seepage–Temperature Field for Earth Dam Using Experimental Test

Yu Wang[1], **Yanchang Gu**[2], **Shijun Wang**[2] **and Xiangbao Duan**[2]

[1]*College of Civil Engineering, Jiangsu Open University, No. 399, the North Road of Jiangdong, Nanjing, Jiangsu, China*
[2]*Nanjing Hydraulic Research Institute, No. 223, Guangzhou Road, Nanjing, Jiangsu, China*

Correspondence should be addressed to Yu Wang; wangyu@jsou.edu.cn

Received 26 April 2023; Revised 18 July 2023; Accepted 28 July 2023; Published 11 August 2023

Academic Editor: Said El Kafhali

Monitoring the seepage field is essential to characterize the operation of the earth dam. However, conventional seepage monitoring typically involves the use of a piezometer tube or pressure sensor for point distribution. A mathematical model incorporating the feedback of the temperature field on the seepage field was proposed based on experimental test observations. First, a theoretical analysis of the mathematical model is conducted, which includes examining the relationship between the variation of temperature field and factors, such as hydraulic gradient, water and soil temperature difference, hydraulic conductivity, thermal conductivity, specific heat, and time. Second, a homogeneous earth dam model is constructed in the laboratory with a distributed temperature sensor system to obtain synchronous information of the seepage–temperature field. Finally, the parameters of the mathematical model are quantified using observations from experimental tests, demonstrating good agreement between calculated and measured values. The experimental results indicate the feasibility of inferring seepage field monitoring information from the temperature field and elucidation of the interaction mechanism of the coupled fields. The quantitative mathematical model of the temperature field feedback on the seepage field is validated for its applicability in earth dams.

1. Introduction

Engineering projects have become progressively more complex in recent decades, encompassing the development of various energy sources, such as oil, natural gas, geothermal, and others, the construction of large dams for water conservation, the excavation of deep tunnels in the earth, the storage of nuclear waste, and the mitigation of pollutants in environmental projects [1–3]. These intricate engineering practices have led to the evolution of single-field studies toward the coupling of two or more fields, such as temperature field, seepage field, and deformation field [4]. As a result, it is crucial to elucidate the interaction mechanisms in these coupled fields in order to ensure the safe operation of the engineering projects.

Seepage, as an environmental factor affecting geological bodies, has significant implications for soil deformation and structural stability. In the case of earth dams, seepage represents a major hazard that can compromise their safety. In fact, studies have shown that 52.5% of earth dam accidents worldwide are attributed to piping and leakage [5]. About 60% of more than 30,000 endangered earth dams have seepage problems in China [6]. The seepage field of an earth dam refers to the spatial region occupied by the equipotential lines of the water head and the percolation flow lines. At any given point within the seepage field, there exists a specific water head and seepage velocity, which are functions of the coordinates and time of the respective points [7–9]. However, due to the complexity of the seepage field, traditional monitoring methods for earth dams are limited to local observations at a few typical sections using the piezometric tubes or pore pressure sensors. This approach may not capture seepage events at discrete points, leading to potential hidden hazards, such as piping, heave, concentrated leaks, and contact erosion, among others, that could threaten the integrity of earth dams.

The rapid advancements in fiber sensing technology have led to the recognition of the potential of distributed temperature sensors (DTS) for seepage monitoring [10]. DTS operates based on the principles of fiber Raman scattering and optical time-domain reflection, allowing for precise and

accurate temperature measurements along the fiber length. Specifically, a laser pulse signal of specific energy and width is injected into the fiber, and the resulting scattered signal generated during fiber transmission is continuous [11]. By analyzing the time interval between the intensity of the back-scattered light wave and the signal of the incident optical pulse, the temperature field information of the scattered point can be demodulated to obtain the temperature profile of the entire fiber [12–14]. It has been reported that the temperature field and the seepage field in earth dams are interrelated, with mutual interactions and influences [15]. Ghafoori et al. [16, 17] developed a laboratory-scaled model to continuously monitor seepage by a passive optical fiber DTS system. In addition, the water temperature upstream of the dam may vary periodically with the seasonal changes. If the permeability of the soil is small, the temperature in the dam body is essentially constant with the season. However, if the soil permeability is high, the temperature within the dam body may significantly change with the seasonal variations, with annual temperature variations ranging from 5 to 10°C [18, 19]. Therefore, the spatial distribution of the temperature field and the time-series data of the temperature at the measuring point can be utilized to analyze the distribution of the seepage field. The DTS can be considered a suitable measurement tool for monitoring the seepage field in earth dams even if the measuring points of the earth dam are distributed far apart.

DTS offers several advantages, including small size, continuous monitoring, good flexibility, high measuring precision, and the ability to operate in harsh environments [20–22]. As a result, various fiber-optic temperature monitoring systems have been developed and widely used for seepage monitoring worldwide. For example, Barrias et al. [23] developed a multichannel fiber-optic temperature sensor system using an optical time domain reflectometer for temperature measurements. Xiang and Wang [24] used DTS to analyze long-term temperature data from a buried pipe in a dam body to assess the seepage condition of an earth dam. Li et al. [25] constructed a simplified mathematical model to describe the coupling between the seepage field and the temperature field, considering different fiber arrangements and proximity of temperature measurements. In China, DTS technology has been successfully applied to the seepage monitoring of many major water conservancy projects, including the Three Gorges Dam, Xiaowan Arch Concrete Dam, Si Anjiang Concrete Face Rockfill Dam, and Changtiao Hydropower Station [26].

However, the current application of DTS technique is limited to qualitative determination of leak location for earth dams, and the existing mathematical models are only able to provide qualitative identification. Hence, there is a need to develop a mathematical model that utilizes quantitative parameters to establish a feedback mechanism between the temperature field and the seepage field, enabling accurate identification of seepage hazards.

In this study, the relationship between the variation of temperature field and hydraulic gradient, water and soil temperature difference, hydraulic conductivity, thermal conductivity, specific heat, and time was analyzed theoretically to build a mathematical model. Laboratory physical model tests were then conducted to validate the feasibility of the proposed mathematical model, using observations from DTS and piezometer tubes. The objective of this research is to develop a quantitative mathematical model that can reveal the interaction mechanism of the coupled fields for earth dams by incorporating the temperature field as a feedback mechanism for seepage monitoring.

2. Materials and Methods

2.1. Analytical Method. The temperature fluctuations at a specific point within the dam body due to seepage are influenced by several factors, including the hydraulic gradient, the difference between the water temperature and the soil temperature, the hydraulic conductivity, the thermal conductivity coefficient, the specific heat, and time. The temperature variation can be described as follows:

$$\Delta T = F(J, T_{ws}, k, \lambda, C, t), \tag{1}$$

where ΔT is the temperature variation, J is the hydraulic gradient, T_{ws} is the difference between the water temperature and the soil temperature, k is the hydraulic conductivity, λ is the thermal conductivity coefficient, C is the specific heat, and t is the time.

Assuming that the seepage of homogeneous soil conforms to Darcy's law, it should be noted that in a homogeneous earth dam with stable seepage, the hydraulic conductivity, the thermal conductivity coefficient, and the specific heat can be treated as constants [27]. Hence, the hydraulic gradient, the difference between the water temperature and the soil temperature, and time are the key factors that impact temperature variations in different regions of the dam.

The mathematical model for the temperature field of the dam body under the influence of the seepage field can be expressed as follows:

$$\left(\lambda\frac{\partial T^2}{\partial x^2} + \lambda\frac{\partial T^2}{\partial y^2}\right) + C_w\rho_w\left[\frac{\partial(v_x T)}{\partial x} + \frac{\partial(v_y T)}{\partial y}\right] + Q = C\rho\frac{\partial T}{\partial t}, \tag{2}$$

where x, y are the coordinates of the measuring point, ρ_w, ρ is the density of water and soil, C_w, C are the specific heat of water and soil, and v_x, v_y are the seepage velocity of the x direction and the y direction, respectively. $(\lambda\partial T^2/\partial x^2 + \lambda\partial T^2/\partial y^2)$ in Equation (2) represents the heat introduced by dam body, $C_w\rho_w[\partial(v_x T)/\partial x + \partial(v_y T)/\partial y]$ refers to the heat carried away or left behind by water flowing in and out of dam body, and Q is the heat source inside dam body

It is assumed that the heat introduction effect and other heat sources inside the dam body are not considered, Equation (2) can be simplified as follows:

$$C\rho\frac{\partial T}{\partial t}\propto C_w\rho_w\left[\frac{\partial(v_xT)}{\partial x}+\frac{\partial(v_yT)}{\partial y}\right]. \quad (3)$$

Equation (3) emphasizes primarily that the temperature variation of the dam body is proportional to the heat carried away or left behind by seepage.

Assuming the seepage flow obeys Darcy law:

$$v_x = kJ_x, \quad (4)$$

$$v_y = kJ_y, \quad (5)$$

where J_x, J_y are the hydraulic gradients of the x-direction and the y-direction, respectively.

Substituting Equations (4) and (5) into Equation (3), subsequent integrating results in Equation (6):

$$C\rho\Delta T(t)\propto C_w\rho_w k\left[J_xG_1(t)+J_yG_2(t)\right], \quad (6)$$

where $G_i(t)$ is the time-dependent integration variable.

Equation (6) indicates that a higher hydraulic gradient results in faster temperature changes, indicating a positive correlation between temperature variation and hydraulic gradient at the measuring point. Notably, the rate of temperature variation is positively correlated with the specific heat of water but inversely correlated with the specific heat of soil.

Furthermore, the temperature at a point in the soil is mixture combination of the water temperature from seepage and the temperature of the soil particles [28]. It is evident that a larger temperature difference between the water and soil temperatures leads to faster changes in the measured soil temperature [29]. In the laboratory model of the earth dam, the reservoir water seeps from the upstream surface to the downstream surface, resulting in a gradual decrease in temperature. As the temperature difference between water and soil decreases from large to small, the rate of heat transfer at the heat flow front slows down. This implies that the temperature change in the dam body is negatively correlated with the distance from a specific point to the upstream surface. To reflect this phenomenon, it is expressed in terms of the system coordinates in the established model, as shown in Equation (7):

$$\Delta T(t)\propto T_{ws} = \Phi(x,y), \quad (7)$$

where $\Phi(x,y)$ is the function of the system coordinates established by the physical model.

Based on the process line distribution of temperature change at typical measurement points, the temperature change is related to time as follows:

$$\Delta T(t) = b_1'\theta(t) + b_2'\ln\theta(t), \quad (8)$$

where $\theta(t)$ is the time difference between the observation time t_i and the initial time t_0 (min) multiplied by 0.01, and b_1', b_2' are the undetermined coefficients.

Considering the uniformity of the dam and the continuity of the temperature field distribution, the hydraulic gradient and the time factor were combined with the coordinate function, respectively. Therefore, when Equations (6)–(8) are combined, it results in a mathematical model that reflects the feedback of the seepage field from temperature field in a homogeneous earth dam.

$$\Delta T(x,y,t) = a_0 + J(x,y)\Phi_1 + \theta\Phi_2 + \ln(\theta)\Phi_3, \quad (9)$$

where a_0 is the constant, $J(x,y)$ is the hydraulic gradient of the measuring point, and Φ_i is the expression of the system coordinate.

$$\Phi_i = b_{i0} + b_{i1}x + b_{i2}y + b_{i3}x^2 + b_{i4}y^2 + b_{i5}xy \quad i = 1,2,3. \quad (10)$$

Then,

$$J(x,y) = \frac{\Delta T(x,y,t) - (a_0 + \theta\Phi_2 + \ln(\theta)\Phi_3)}{\Phi_1}, \quad (11)$$

where $t \geq t_0, (x,y) \in \Omega$. The initial condition is that $T(x,y,t_0) = T_0(x,y)$, and $T_0(x,y)$ refers to the initial distribution of temperature field at time t_0.

The heat flow boundaries are described by the Dirichlet and Neumann boundary condition types. In the Dirichlet type, a known temperature T_D is prescribed on the boundary domain $\Gamma_{BT} \subset \Gamma$ and time t [16]:

$$T(x,t) = T_D(t) \text{ on } \Gamma_{BT} \times t[t_0,\infty). \quad (12)$$

The Neumann-type boundary condition for the heat transfer can be described by Equation (13):

$$q(x,t) = q_{DT}(t) \text{ on } \Gamma_{Bq} \times t[t_0,\infty), \quad (13)$$

where q_T is the heat flux across the boundary Γ_{Bq}, and q_{DT} is the prescribed Neumann heat flux.

Equation (11) represents a mathematical model reflecting hydraulic gradient at any point by measuring the distribution of the temperature field of earth dam. The seepage velocity can be deduced using Equations (4) and (5).

2.2. Physical Model Test. The main objective of the physical test is to examine the spatial distribution of the seepage field and the temperature field and to quantitatively validate the feasibility of the mathematical model. In order to carefully observe the coupled effect of the seepage field and the temperature field, the use of standard sand, which is a highly permeable material, is chosen for the earth dam. The dam body in the physical test is filled with homogeneous fine sand. It is important to note that this test is only applicable to low-velocity laminar flows in homogeneous soils not to high-velocity turbulent flows. In addition, factors such as the density and hydraulic conductivity of the sample, as well as

Table 1: The material characteristics.

Soil type	Dry density, ρ_d (g/cm^3)	Porosity, n	Hydraulic conductivity, k (cm/s)	Uniformity coefficient, C_u
Fine sand	1.70	0.32	5×10^{-3}	3.23

Figure 1: Physical model of earth dam.

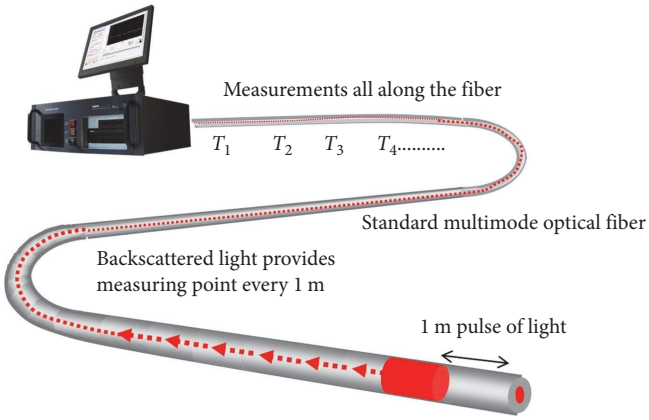

Figure 2: The schematic of Sentinel DTS.

the accuracy and sensitivity of the instrument, can be potential sources of error during sample preparation and measurement. The specific heat of fine sand is 1,200 J/kg/°C and water is 4,200 J/kg/°C. The other physical parameters are shown in Table 1. The top of the earth dam was 30 cm wide, the bottom was 240 cm wide and 70 cm high. Both the upstream and downstream slopes were 1 : 1.5. The earth dam was laid in a sink, where the sides were plexiglass, the bottom was a plate of steel, and the top was open. Grid lines were drawn on the surface of the plexiglass to establish the coordinates for various measuring points, as shown in Figure 1.

Sentinel DTS, manufactured by Sensornet of the United Kingdom, was used in the physical model test. The temperature resolution was 0.01°C, the accuracy was 0.1°C, and the spatial resolution was 1.0 m, which met the requirement of technical performance index of the test, as shown in Figure 2. Once the fiber was laid inside the dam, the distribution of the temperature field was obtained, allowing for feedback on the distribution of seepage field. However, in smaller physical model tests, accurate temperature measurement at a specific point would be impossible if the fiber was linearly tiled. Therefore, a fixed length of fiber was used to measure the temperature at a designated point in the model. In this case, a bundle of 3 m fibers was used as a measurement point to measure the temperature of the earth dam.

In this test, the fiber bundles were arranged with a horizontal spacing of 30 cm and a vertical spacing of 10 cm. To avoid direct contact between the optical fiber and the bottom plate of the sink, a 5 cm thick sand sample was set on the bottom plate of the sink before laying the first layer of optical fiber. The first bundle of fibers was laid at the inlet of the sink, and after laying out eight bundles of fibers, the sand was filled to a height of 10 cm and then smoothed and compacted. The second layer of optical fiber was laid from the tail of the sink to the inlet, followed by sand compaction and so on, until a 70 cm high earth dam was formed in the common direction of the sink. In total, six layers and 33 fiber bundles were laid to obtain temperatures at 33 measuring points inside the dam. The dots in Figure 3 represent the locations of distributed fibers.

The upstream water level of the dam body was set at 60 cm, and the temperature of water remained at 40°C. However, there was no water downstream, and the ambient temperature in the laboratory was 17.48°C. The water tank was heated to ~70°C, and then the proper proportion of hot water and tap water were mixed into the sink using the submersible pump. The upstream water level was kept steady at 60 cm throughout the test, meaning that the upstream water level remained constant as the upstream water started to percolate through the dam until steady seepage developed. In addition, the distributed fiber temperature measurements were performed in 1 min intervals and lasted for 360 min. Simultaneously, the water level of the piezometer tube and the quantity of seepage from the dam were observed every 10 min. Three samples of seepage quantity were recorded at a time, with a fixed amount of water used for each observation.

3. Results

The results depicting the equipotential lines of the seepage field at different times are shown in Figure 4, with a time interval of 60 min. In the figure, the blue region represents the saturated soil, while the upper region indicates the unsaturated soil, with the dividing line being the phreatic line where the pore pressure is zero. As evident in Figure 4(a)–4(d), during the first 240 min, the water head distribution of the seepage field changes slightly and gradually stabilizes. This can be attributed to the homogeneous nature of the fine sand and the steady upstream water level, which results in a steady percolation flow through the earth dam and nearly identical head losses. These results are consistent with Darcy law, which is applicable only to such linear, laminar flow.

The results for the equipotential lines of the temperature field at different times are shown in Figure 5 for a time interval of 60 min. The temperature contours of the earth dam exhibit a right bracket-shape distribution, indicating

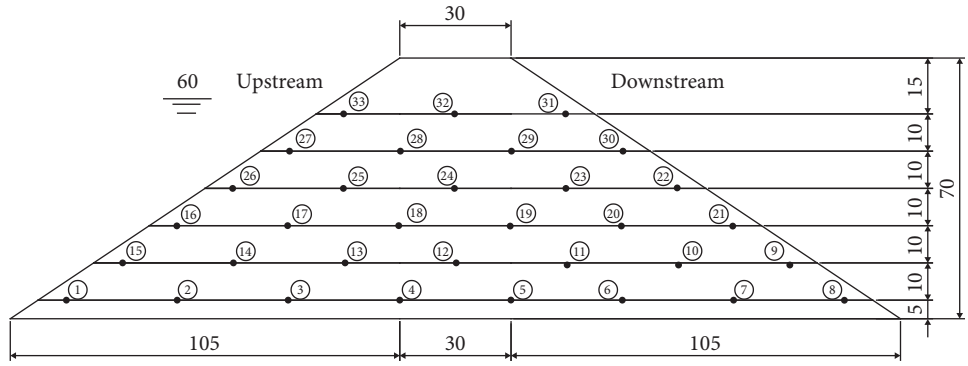

Figure 3: Distributed fiber location.

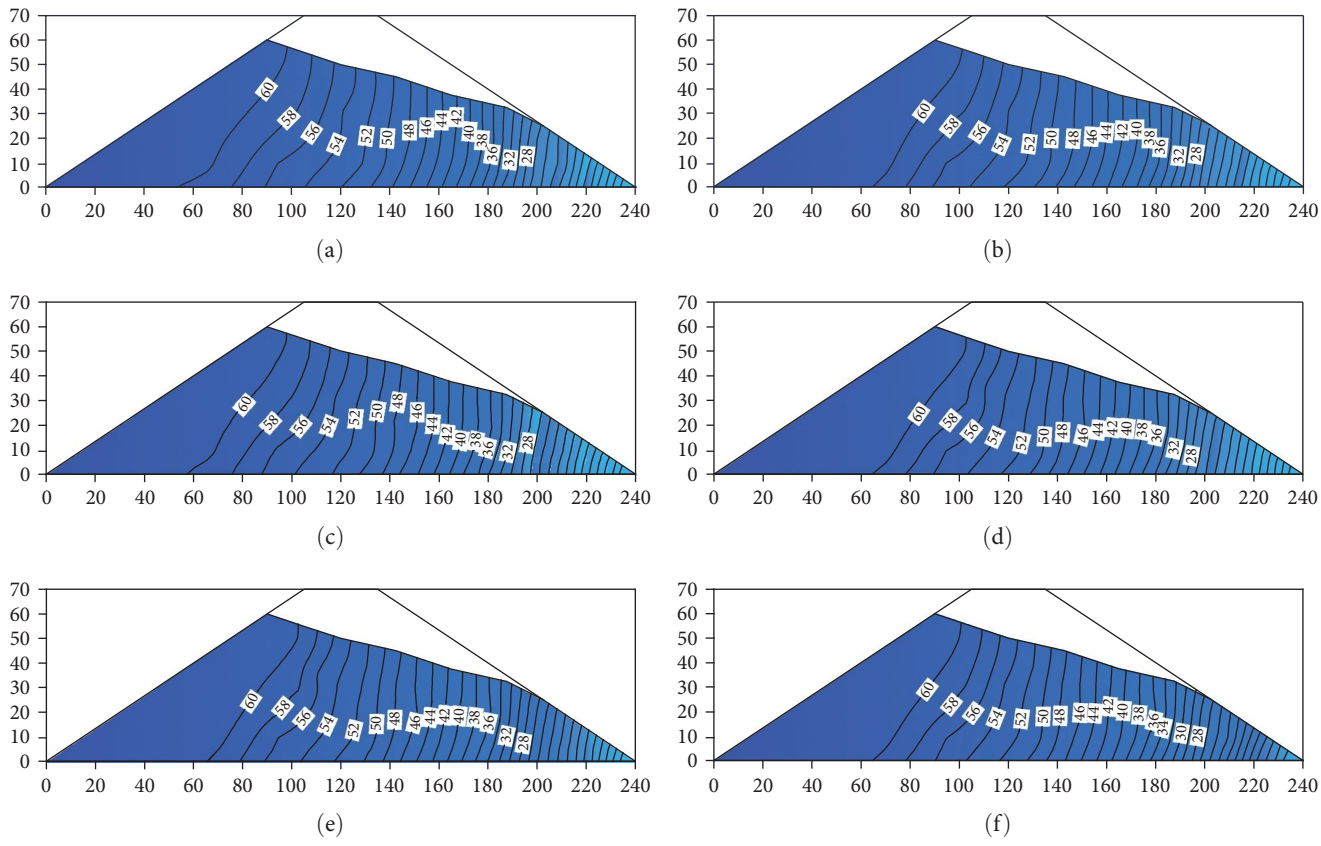

Figure 4: Equipotential line of seepage field at different times: (a) $t = 60$ min, (b) $t = 120$ min, (c) $t = 180$ min, (d) $t = 240$ min, (e) $t = 300$ min, and (f) $t = 360$ min.

that the temperature in the middle of the dam is higher than the temperature at the top and bottom of the same vertical section. With the passage of time, the isotherm gradually moves downstream, and the distribution of temperature contours changes from dense to sparse. The velocity of motion at the center of the isotherm is significantly larger than that at the base of the isotherm. This is most likely due to the longer percolation diameter of the bottom plate and the heat dissipation in the steel plate. Moreover, the curvature of the downstream slope temperature contour increases, with the 23°C temperature contour becoming smaller as it moves downstream. This is caused by the seepage flow of the dam body not only moving horizontally but also vertically downward, resulting in a smaller height of the percolation section.

4. Discussion

4.1. Determination of Mathematical Model Parameters. In order to determine the parameters in Equation (9), experimental data from the physical model were used to quantify the mathematical model. In Figure 3, the temperature data were obtained for 33 measuring points in the physical model test. Points 3 and 17, which had poor observational data, were eliminated, and points 22, 30, 31, and 32 above the

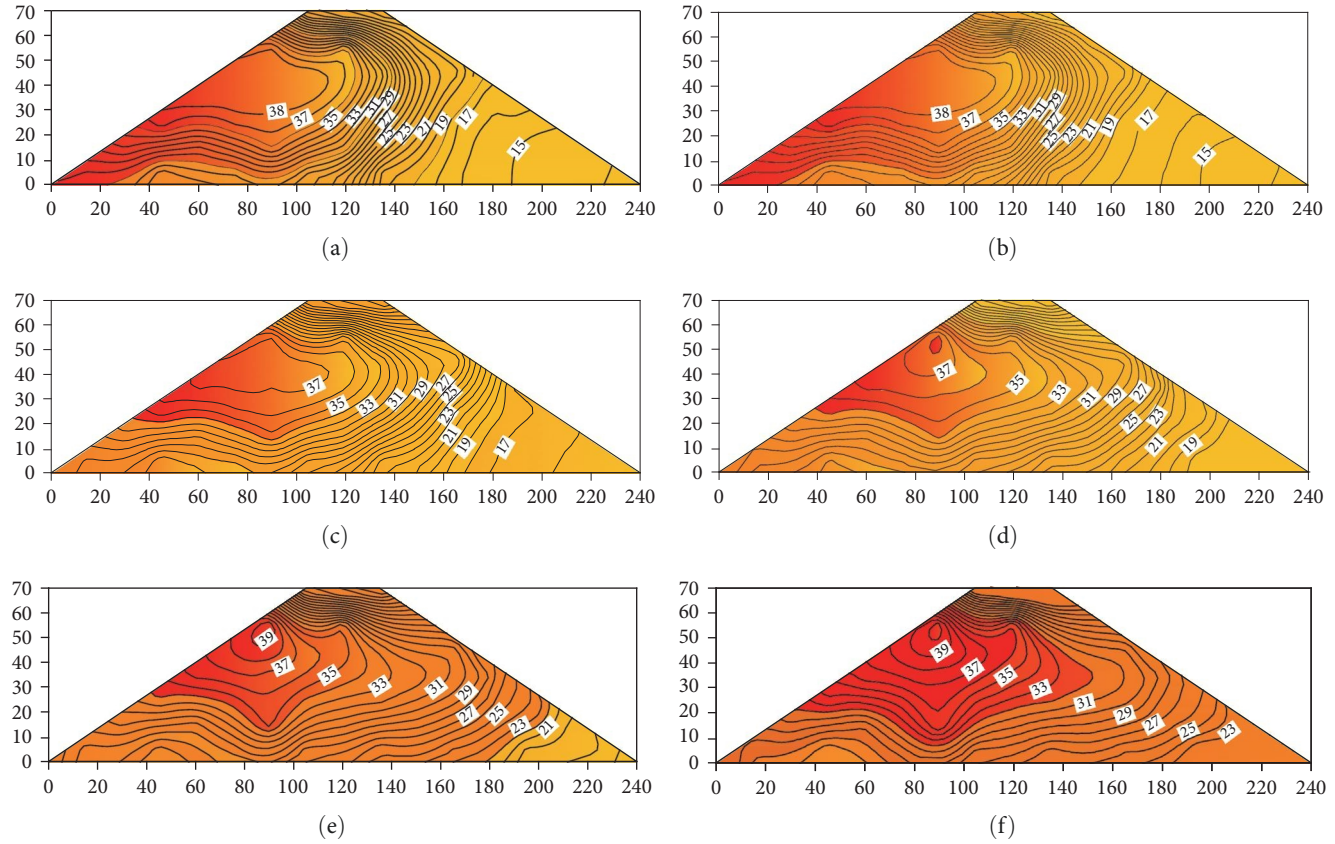

Figure 5: Equipotential line of temperature field at different times: (a) $t = 60$ min, (b) $t = 120$ min, (c) $t = 180$ min, (d) $t = 240$ min, (e) $t = 300$ min, and (f) $t = 360$ min.

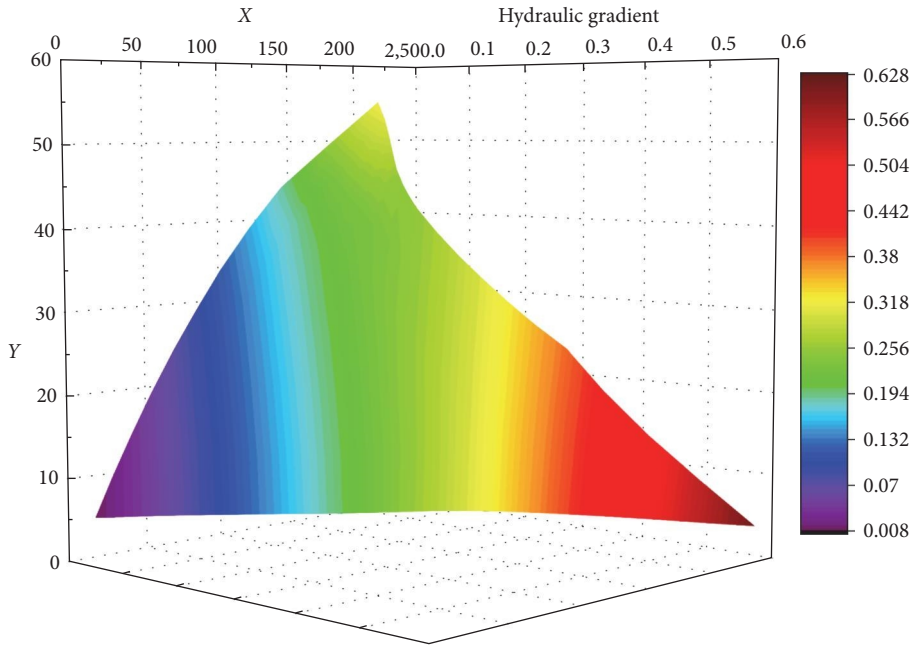

Figure 6: Spatial distribution of hydraulic gradients.

phreatic line were not considered. Moreover, points 9 and 19 were reserved for the verification of the reliability of the physical model. The coordinates and hydraulic gradients for the remaining 25 points are shown in Figure 6 and Table 2. The time series ranges from 183 to 423 min, with measurements taken at 10 min intervals.

The stepwise regression method was used to determine the undetermined coefficients of Equation (9) based on the

Table 2: Coordinates and hydraulic gradients at measuring points.

Point	x	y	J
1	15	5	0.009
2	45	5	0.055
4	105	5	0.191
5	135	5	0.249
6	165	5	0.311
7	195	5	0.439
8	225	5	0.627
10	180	15	0.356
11	150	15	0.274
12	120	15	0.224
13	90	15	0.165
14	60	15	0.091
15	30	15	0.033
16	45	25	0.067
18	105	25	0.205
20	165	25	0.300
21	195	25	0.384
23	150	35	0.262
24	120	35	0.236
25	90	35	0.195
26	60	35	0.113
27	75	45	0.179
28	105	45	0.245
29	135	45	0.236
33	90	55	0.322

observational data. The stepwise regression method automatically selects the most important variables from a large number of available variables and builds a predictive model for the regression analysis. The stepwise regression method was employed, wherein independent variables were introduced one by one with the condition that their partial regression sum of squares was significant after testing. Simultaneously, after introducing a new independent variable, the old independent variables were tested one by one, and any insignificant variables were eliminated. This process was repeated until no new variables were introduced and no old variables are removed. For the homogeneous earth dam, the resulting mathematical model exhibited a complex correlation coefficient of 0.96 with a residual standard deviation of 1.41. A significance level of 0.01 was used to test the regression model. The statistical value F of this test was 763.52, which was well above the critical value $F(18,606)$ of 1.99. The correlation coefficient and the standard deviation of the residuals do not change much, but the value of the statistic F increases significantly and is much larger than the critical value, so the mathematical model predicts better. More information about the specific criteria for variable selection is available in literature [30].

$$\Delta T = 18.233 + J(59.823 - 1.249x + 2.966y + 0.004x^2 - 0.022xy) + \ln(\theta)(-5.925 + 0.16y - 0.007y^2 + 0.003xy). \quad (14)$$

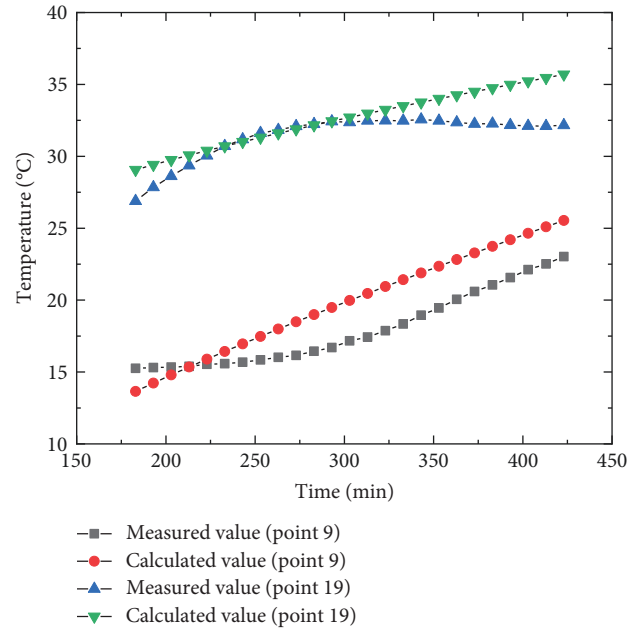

Figure 7: Temperature variation of measured and calculated values at points 9 and 19.

4.2. Verification of Physical Model. The calculated values in Equation (14) were compared with measured values obtained from the distributed optical fiber at points 9 and 19 at different times, as shown in Figure 7 and Table 3. The comparison revealed that the calculated and measured values are in good agreement overall. At point 19, the mean square error was only 2.84%, while at point 9, the mean square error was 5.36%, possibly due to fewer sampling points downstream than upstream. Nevertheless, the overall reliability of the model has been verified through this comparison.

Equation (11) provides the means to determine the hydraulic gradient by obtaining the coordinates of the point, the time, and the corresponding temperature change. For example, although the calculated values of the hydraulic gradient at point 19 are not the same at different times, the relative errors are generally within 10%, which is close to the measured value of 0.25, as shown in Figure 8 and Table 4. This indicates that the hydraulic gradient at the measuring point of the homogeneous earth dam can be quantitatively predicted by the feedback mathematical model based on Equation (14). Furthermore, the seepage velocity can be also calculated using Equations (4) and (5). By analogy, mathematical models of the temperature field feeding back the seepage field can be established under different operating conditions.

4.3. Analysis of Coupled Mechanism. The interaction between the seepage field and the temperature field in the dam body leads to a coupled and dynamic equilibrium state, where the seepage field is influenced by the temperature field, and the temperature field is influenced by the seepage field. This mutual interaction results in a complex and dynamic relationship between the two fields. The coupling process

Table 3: Temperature errors of measured and calculated values at points 9 and 19.

Time (min)	Point 9			Point 19		
	Measured value (°C)	Calculated value (°C)	Error (%)	Measured value (°C)	Calculated value (°C)	Error (%)
183	15.26	13.65	10.50	26.89	29.06	8.07
193	15.31	14.23	7.04	27.85	29.41	5.62
203	15.34	14.80	3.53	28.62	29.75	3.93
213	15.39	15.35	0.29	29.36	30.08	2.44
223	15.54	15.89	2.30	30.05	30.39	1.16
233	15.58	16.43	5.45	30.71	30.71	0.01
243	15.68	16.96	8.14	31.17	31.01	0.53
253	15.85	17.48	10.29	31.62	31.31	0.98
263	16.02	17.99	12.29	31.83	31.60	0.74
273	16.16	18.49	14.48	32.10	31.88	0.66
283	16.44	18.99	15.53	32.24	32.16	0.25
293	16.70	19.49	16.67	32.43	32.44	0.04
303	17.17	19.98	16.38	32.37	32.71	1.06
313	17.43	20.46	17.39	32.48	32.98	1.54
323	17.88	20.94	17.16	32.49	33.24	2.32
333	18.34	21.42	16.78	32.48	33.50	3.15
343	18.95	21.89	15.53	32.56	33.75	3.67
353	19.45	22.36	14.93	32.48	34.01	4.70
363	20.05	22.82	13.81	32.36	34.27	5.86
373	20.60	23.28	13.04	32.26	34.50	6.95
383	21.06	23.74	12.74	32.27	34.75	7.66
393	21.56	24.20	12.20	32.17	34.99	8.76
403	22.12	24.65	11.44	32.11	35.22	9.68
413	22.52	25.10	11.46	32.10	35.46	10.45
423	23.03	25.54	10.93	32.16	35.69	10.98
	Mean square error: 5.36			Mean square error: 2.84		

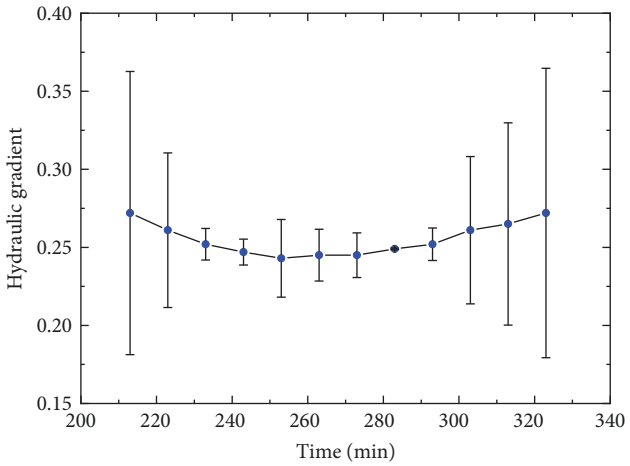

Figure 8: Error bar of calculated values at point 19.

between the temperature field and the percolation field is a process of dynamical change of the thermal energy and fluid in the medium. Any instability in one field can cause changes in the other field. On the one hand, a change in the seepage field of an earth dam will allow the seepage flow to participate in the heat transfer and exchange of soil, which affects the distribution of the temperature field. On the other hand,

Table 4: The calculated values of the hydraulic gradient at point 19.

Time (min)	213	223	233	243	253	263
Hydraulic gradient	0.272	0.261	0.252	0.247	0.243	0.245
Error (%)	9.07	4.95	1.01	0.83	2.49	1.66
Time (min)	273	283	293	303	313	323
Hydraulic gradient	0.245	0.249	0.252	0.261	0.265	0.272
Error (%)	1.43	0.05	1.04	4.72	6.48	9.27

the temperature gradient formed by the variation of the temperature field of the earth dam causes the movement of the percolating water and thus changes the permeability of the soil.

From a physical perspective, heat is exchanged through medium contacts, while the seepage diffuses and flows in the pores of the porous medium due to the potential energy difference. At the same time, fluid also serves as the medium for heat propagation, carrying heat along the track lines through seepage in the porous medium. Additionally, changes in thermal energy can alter the physicochemical properties of the medium and the fluid, affecting medium and fluid volume effects, as well as characteristic parameters of the fluid. Therefore, the coupling between the temperature field and the seepage field involves energy balance, dissipation processes, as well as physical reactions within the medium.

5. Conclusions

A mathematical model was proposed to quantitatively study the coupling between the temperature field and the seepage field. The reliability of the mathematical model was verified through observations of the physical model. The main conclusions are as follows:

(1) The relationship between temperature variation, hydraulic gradient, temperature difference between seepage water and soil, hydraulic conductivity, thermal conductivity, specific heat, and time was derived based on theoretical analysis, leading to the development of a mathematical model for the feedback of the temperature field to the seepage field in a homogeneous earth dam.

(2) The parameters of the mathematical model for the seepage field, which is fed back from the temperature field, were determined through the observations of the physical model test. The stepwise regression method was used to ensure the accuracy of the mathematical model.

(3) The hydraulic gradients calculated from the mathematical model are verified by the physical model test. The use of distributed temperature sensor systems to infer seepage information was found to be feasible, providing a new approach for quantitative monitoring of the distribution of seepage in earth dams.

The mathematical model provides a deeper understanding of the coupling mechanism of the seepage–temperature field for an earth dam. The methods and results may be of interest to hydrologists, mathematicians, and water engineers who focus on groundwater. This mathematical model is currently limited to stable laminar flow through a homogeneous earth dam and requires testing in engineering practice. Further studies involving models with different types of soils under complex geological conditions and nonlaminar flow regimes should be more considered.

Data Availability

The data used to support the findings of this study are included within the article.

Conflicts of Interest

The authors declare that they have no conflicts of interest.

Acknowledgments

This research was backed up by the National Natural Science Foundation of China (grant number 51979175), the General Project of Philosophy and Social Science Research in Jiangsu Universities (grant number 2022SJYB0841), and the Course Innovation and Optimization Plan (grant number 1028154ZL2023/004).

References

[1] Y. Wang, X. B. Duan, Y. C. Gu, and S. J. Wang, "Experimental investigation of the seepage-induced failure process in granular soils," *Geofluids*, vol. 2022, Article ID 5703151, 17 pages, 2022.

[2] T. L. Wahl, K. W. Frizell, and H. T. Falvey, "Uplift pressures below spillway chute slabs at unvented open offset joints," *Journal of Hydraulic Engineering*, vol. 145, no. 11, Article ID 04019039, 2019.

[3] D. M. Gu, D. Huang, H. L. Liu, W. G. Zhang, and X. C. Gao, "A DEM-based approach for modeling the evolution process of seepage-induced erosion in clayey sand," *Acta Geotechnica*, vol. 14, no. 6, pp. 1629–1641, 2019.

[4] Y. Wang, X. Duan, Y. Gu, and S. Wang, "Fractal characteristics of the seepage erosion process in porous soil," *Geofluids*, vol. 2022, Article ID 3383773, 12 pages, 2022.

[5] D. Ma, H. Y. Duan, J. X. Zhang, X. J. Feng, and Y. L. Huang, "Experimental investigation of creep-erosion coupling mechanical properties of water inrush hazards in fault fracture rock masses," *Chinese Journal of Rock Mechanics and Engineering*, vol. 40, no. 9, pp. 1751–1763, 2021.

[6] L.-L. Zeng, Y.-Q. Cai, Y.-J. Cui, and Z.-S. Hong, "Hydraulic conductivity of reconstituted clays based on intrinsic compression," *Geotechnique*, vol. 70, no. 3, pp. 268–275, 2020.

[7] H. J. Kima, H. Byuna, Y. B. Songa et al., "Multi-channel fiber-optic temperature sensor system using an optical timedomain reflectometer," *Results in Physics*, vol. 11, pp. 743–748, 2018.

[8] R.-H. Wang, P.-G. Sun, D.-Q. Li, A. Tyagi, and Y. Liu, "Three-dimensional seepage investigation of riverside tunnel construction considering heterogeneous permeability," *ASCE-ASME Journal of Risk and Uncertainty in Engineering Systems, Part A: Civil Engineering*, vol. 7, no. 4, Article ID 04021041, 2021.

[9] R.-H. Wang, D.-Q. Li, M.-Y. Wang, and Y. Liu, "Deterministic and probabilistic investigations of piping occurrence during tunneling through spatially variable soils," *ASCE-ASME Journal of Risk and Uncertainty in Engineering Systems, Part A: Civil Engineering*, vol. 7, no. 2, Article ID 04021009, 2021.

[10] Y. Wang, Y. Liu, and B. Wang, "Experimental study on fractal characteristics of seepage-induced failure in granular soil," *Computational Particle Mechanics*, vol. 10, no. 4, pp. 1–15, 2023.

[11] J. S. Wu, H. U. DeZhi, L. I. Wenjun, and C. A. I. Xin, "A review on non-Darcy flow-forcheimer equation, hydraulic radius model, fractal model and experiment," *Fractals*, vol. 24, no. 2, Article ID 1630001, 13 pages, 2016.

[12] D. Zhu, D. V. Griffiths, and G. A. Fenton, "Worst-case spatial correlation length in probabilistic slope stability analysis," *Geotechnique*, vol. 69, no. 1, pp. 85–88, 2019.

[13] A. A. Ahmed, "Saturated–unsaturated flow through leaky dams," *Journal of Geotechnical and Geoenvironmental Engineering*, vol. 134, no. 10, pp. 1564–1568, 2008.

[14] B. Yuan, Z. Li, Z. Su, Q. Luo, M. Chen, and Z. Zhao, "Sensitivity of multistage fill slope based on finite element model," *Advances in Civil Engineering*, vol. 2021, Article ID 6622936, 13 pages, 2021.

[15] F. Zhang, "Mathematical modeling of multiscale network traffic combination prediction based on fuzzy support vector machine," *Mathematical Problems in Engineering*, vol. 2023, Article ID 9972636, 9 pages, 2023.

[16] Y. Ghafoori, M. Maček, A. Vidmar, J. Říha, and A. Kryžanowski, "Analysis of seepage in a laboratory scaled model using passive optical fiber distributed temperature sensor," *Water*, vol. 12, no. 2, Article ID 367, 2020.

[17] Y. Ghafoori, M. Maček, A. Vidmar, J. Říha, and A. Kryžanowski, "Heat transfer by seepage in sand: influence of saturated hydraulic conductivity and porosity," *Acta Hydrotechnica*, vol. 60, no. 34, pp. 1–10, 2021.

[18] J. Ji, Q. Yang, P. Chen, K. Lu, and Y. Wu, "An improved mathematical model of cutting temperature in end milling AI7050 based on the influence of tool geometry parameters and milling parameters," *Mathematical Problems in Engineering*, vol. 2021, Article ID 5705091, 10 pages, 2021.

[19] L. Sheng, D. Ba, and Z. Lu, "Imaging enhancement based on stimulated Brillouin amplification in optical fiber," *Optics Express*, vol. 27, no. 8, pp. 10974–10980, 2019.

[20] Z. Bai, H. Yuan, Z. Liu et al., "Stimulated Brillouin scattering materials, experimental design and applications: a review," *Optical Materials*, vol. 75, pp. 626–645, 2018.

[21] X. Bao and L. Chen, "Recent progress in Brillouin scattering based fiber sensors," *Sensors*, vol. 11, no. 4, pp. 4152–4187, 2011.

[22] L. Sheng, L. Li, L. Liu, L. Hu, M. Yuan, and J. Yan, "Study on the simultaneous distributed measurement of temperature and strain based on Brillouin scattering in dispersion-shifted fiber," *OSA Continuum*, vol. 3, no. 8, pp. 2078–2085, 2020.

[23] A. Barrias, J. R. Casas, and S. Villalba, "A review of distributed optical fiber sensors for civil engineering applications," *Sensors*, vol. 16, no. 5, Article ID 748, 2016.

[24] P. Xiang and H. Wang, "Optical fibre-based sensors for distributed strain monitoring of asphalt pavements," *International Journal of Pavement Engineering*, vol. 19, no. 9, pp. 842–850, 2018.

[25] Y. Li, G. Sun, and X. Wang, "Temperature field-wind velocity field optimum control of greenhouse environment based on CFD model," *Mathematical Problems in Engineering*, vol. 2014, Article ID 949128, 9 pages, 2014.

[26] K. Liu, Z. Lin, D. Cao, and Y. Wei, "Mathematical model for the fluid-gas spontaneous displacement in nanoscale porous media considering the slippage and temperature," *Mathematical Problems in Engineering*, vol. 2018, Article ID 3245498, 8 pages, 2018.

[27] B. Wang, C. Rong, H. Cheng, H. Cai, and S. Zhang, "Analytical solution of steady-state temperature field of single freezing pipe under action of seepage field," *Advances in Civil Engineering*, vol. 2020, Article ID 5902184, 13 pages, 2020.

[28] H. Zhang, B. Zhi, E. Liu, and T. Wang, "Study on varying characteristics of temperature field and moisture field of shallow loess in the freeze-thaw period," *Advances in Materials Science and Engineering*, vol. 2020, Article ID 1690406, 10 pages, 2020.

[29] W. Yu, S. Liu, W. Xu, and D. Wang, "Modal analysis of aeronautic spiral bevel gear in the temperature field," *Journal of Sensors*, vol. 2022, Article ID 1707808, 13 pages, 2022.

[30] Y. Li and J. S. Liu, "Robust variable and interaction selection for logistic regression and general index models," *Journal of the American Statistical Association*, vol. 114, no. 525, pp. 271–286, 2019.